



COLLÈGE  
DE FRANCE  
—1530—

*Chaire de Physique de la Matière Condensée*

# ***Cuprates supraconducteurs : où en est-on ?***

Antoine Georges

Cycle 2010-2011  
Cours 6 – 14/12/2010

# Cours 6 - 14/12/2010

**Cours:** *Phénoménologie de la phase supraconductrice des cuprates (suite)*

## **Séminaire (AG):**

*Progrès théoriques récents*

*(dichotomie noeud/antinoeuds, pseudo-gap) :*

*extensions des méthodes de*

*champ moyen dynamique ("cluster-DMFT")*

- **15h45: Cyril Proust, LNCMI, Toulouse**

*Oscillations quantiques et magnéto-transport dans les cuprates*

- ***Perspectives, conclusions, discussion.***

# I. Energetics of SC transition in underdoped regime: strongly non-BCS !

Key experiments: Groningen, ESPCI/Orsay

## Superconductivity-Induced Transfer of In-Plane Spectral Weight in $\text{Bi}_2\text{Sr}_2\text{CaCu}_2\text{O}_{8+\delta}$

H. J. A. Molegraaf,<sup>1</sup> C. Presura,<sup>1</sup> D. van der Marel,<sup>1\*</sup>  
P. H. Kes,<sup>2</sup> M. Li<sup>2</sup>

Science, 295, 2239 (2002)

EUROPHYSICS LETTERS

15 May 2003

*Europhys. Lett.*, **62** (4), pp. 568–574 (2003)

EPL, 62, 568 (2003)

PRB, 70, 134504 (2004)

### Pairing in cuprates from high-energy electronic states

A. F. SANTANDER-SYRO<sup>1</sup>, R. P. S. M. LOBO<sup>1</sup>, N. BONTEMPS<sup>1(\*)</sup>,  
Z. KONSTANTINOVIC<sup>2</sup>, Z. Z. LI<sup>2</sup> and H. RAFFY<sup>2</sup>

See also: Deutscher, Santander and Bontemps PRB 72, 092504 (2005)

van der Marel et al in "Concepts in electron correlations" (2003); Carbone et al. PRB 74, 064510 (2006)

# Optical conductivity: sum-rules

## 1) Metal in normal state [sketch on board]

‘Low-frequency’ peak: Drude weight (quasiparticles)

‘Intermediate’ frequencies: regime where 1-band model applies

All frequencies: counts all electrons (valence+core)

→ *f-sum rule*: 
$$\int_0^{+\infty} d\omega \sigma_1(\omega) = \frac{\pi n e^2}{2 m} \quad \begin{array}{l} n: \text{all electrons} \\ m: \text{bare mass} \end{array}$$

$$\sigma(\omega) = \sigma_1(\omega) + i\sigma_2(\omega) \quad \text{complex conductivity}$$

*Partial sum-rule over range where 1-band applies:*

$$\int_0^{W_c} d\omega \sigma_1^\alpha(\omega) = -\frac{\pi e^2}{2\hbar^2} a_\alpha^2 K, \quad K \equiv -\sum_k \frac{\partial^2 \varepsilon_k}{\partial k_\alpha^2} n_k$$

If simple TB with n.n hopping:

$$\varepsilon_k = -2t \sum_\alpha \cos k_\alpha \Rightarrow -\frac{\partial^2 \varepsilon_k}{\partial k_\alpha^2} = -2t \cos k_\alpha \rightarrow \text{Kinetic energy}$$

# Energy scales and wavenumbers...

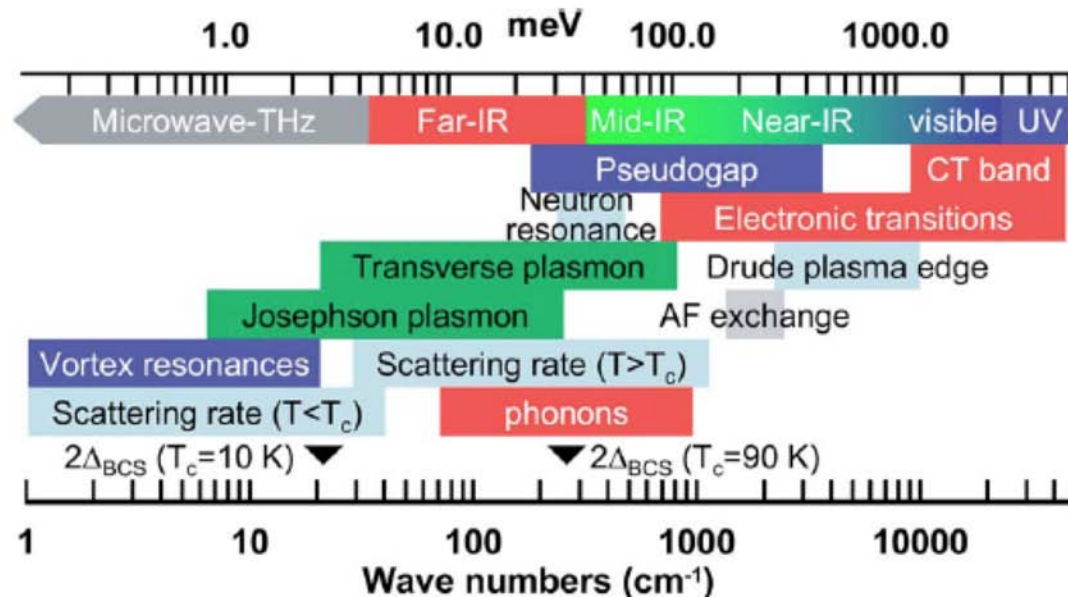


FIG. 6. (Color in online edition) Characteristic energy scales in high- $T_c$  superconductors. Infrared and optical spectroscopies allow one to probe electronic excitations in the frequency range from  $\approx 20 \text{ cm}^{-1}$  to at least  $50\,000 \text{ cm}^{-1}$ . Several other techniques described in this section are suitable for extending the low-energy boundary down to microwave frequencies.

$$8000 \text{ cm}^{-1} = 1 \text{ eV}$$

Note: simple Drude model is both instructive and misleading

$$\frac{d\vec{v}}{dt} = -\frac{e}{m}\vec{E} - \frac{1}{\tau}\vec{v}$$

$$\vec{j} = -ne\vec{v} \Rightarrow \frac{d\vec{j}}{dt} = \frac{ne^2}{m}\vec{E} - \frac{1}{\tau}\vec{j}$$

$$\vec{j}_\omega \equiv \sigma(\omega)\vec{E}_\omega \Rightarrow \sigma(\omega) = \frac{ne^2}{m} \frac{\tau}{1 - i\omega\tau}$$

$$\sigma_1(0) = \frac{ne^2\tau}{m}, \quad \int_0^\infty \sigma_1(\omega)d\omega = \frac{ne^2}{m}$$

[No distinction between valence and core electrons]

[Only structure is Drude peak]

## 2) In the superconducting state

No dissipative term  
for supercurrent !

$$\frac{d\vec{j}_s}{dt} = \frac{n_s e^2}{m^*} \vec{E} \Rightarrow$$
$$\sigma_2(\omega) = \frac{n_s e^2}{m^* \omega} + \sigma_2^{\text{reg}}(\omega)$$
$$\sigma_1(\omega) = \frac{\pi n_s e^2}{2m^*} \delta(\omega) + \sigma_1^{\text{reg}}(\omega)$$
$$= \rho_s \delta(\omega) + \sigma_1^{\text{reg}}(\omega)$$

Ferrell-Glover-Tinkham (FGT) sum-rule:

$$\int_0^\infty d\omega \sigma_1^{\text{SC}}(\omega) \equiv \rho_s + \int_{0^+}^\infty d\omega \sigma_1^{\text{reg}}(\omega) = \frac{ne^2}{m} = \int_0^\infty d\omega \sigma_1^{\text{N}}(\omega)$$

- Total spectral weight is conserved. In usual BCS superconductors, sum-rule is saturated for  $\omega > 4\Delta$
- SC state conductivity always below N state one, difference is in  $\delta$ -function (condensate fraction)

## Experiments: testing sum-rules and energetics

- Need measurement of conductivity over wide frequency range
- High-precision
- Ellipsometry even better (both real and imaginary part)
- Condensed fraction deduced from  $1/\omega^2$  behaviour of  $\varepsilon_1(\omega)$  in very-low frequency range (microwave)

$$\varepsilon(\omega) = \varepsilon_0 + \frac{i}{\omega} \sigma(\omega) \Rightarrow \varepsilon_1^{\text{SC}}(\omega) \sim \frac{\rho_s}{\omega^2} \quad (\omega < \Delta)$$

# Total FGT sum-rule ?

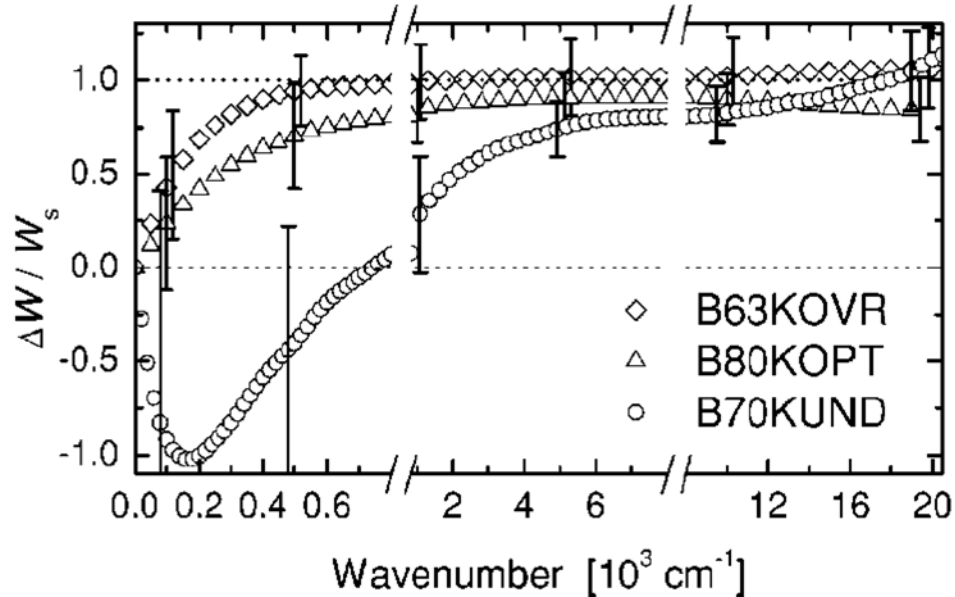
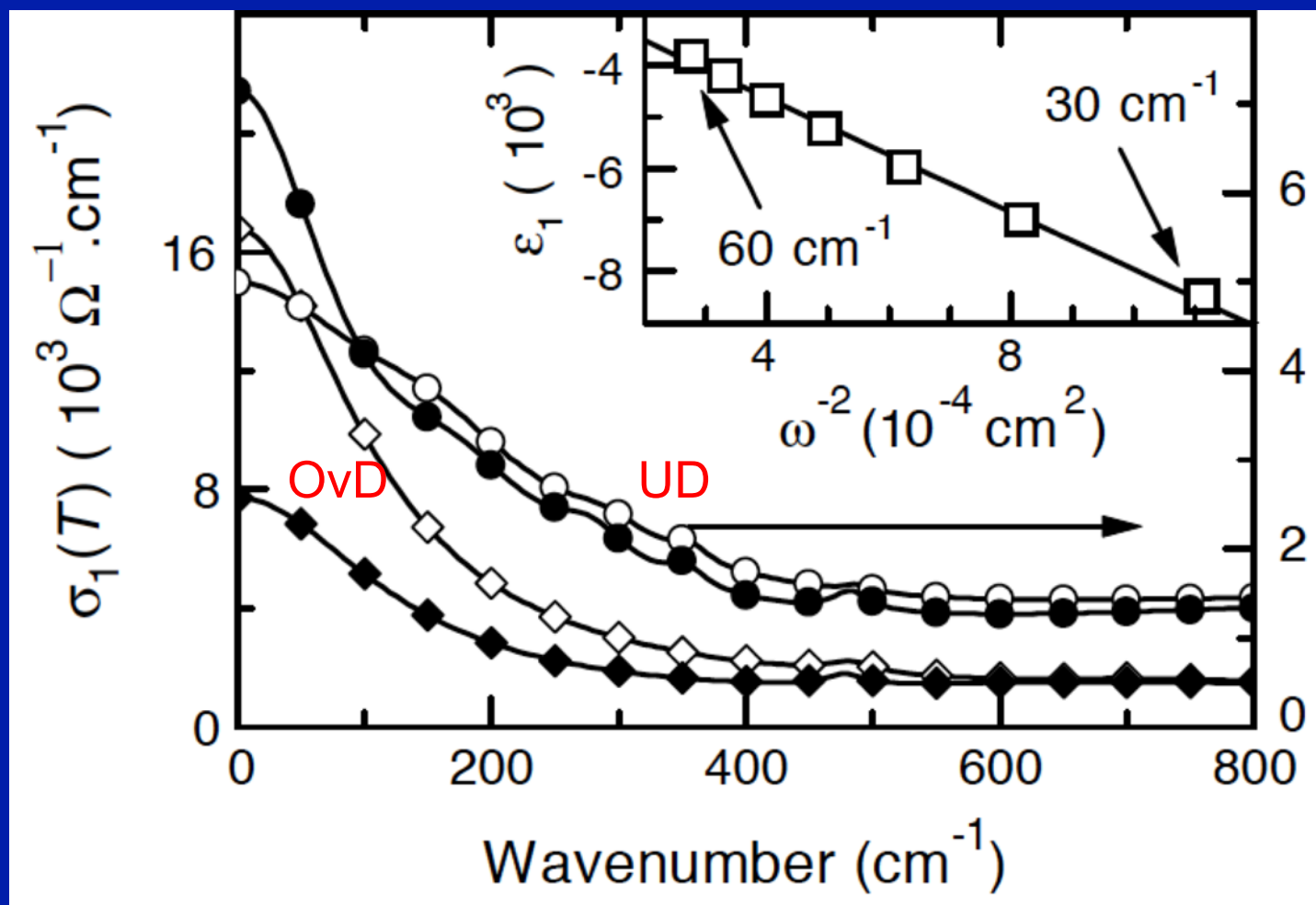


FIG. 5. Ratio  $\Delta W / W_s$  vs frequency showing the exhaustion of the FGT sum rule at conventional energies for the OVR and OPT samples. An unconventional ( $\sim 16\,000 \text{ cm}^{-1}$  or 2 eV) energy scale is required for the UND sample. Note that the frequency scale changes at 800 and 8000  $\text{cm}^{-1}$ . The changes in spectral weight are taken between 80 K–10 K, 91 K–10 K, and 100 K–10 K for the OVR, OPT and UND, samples, respectively.

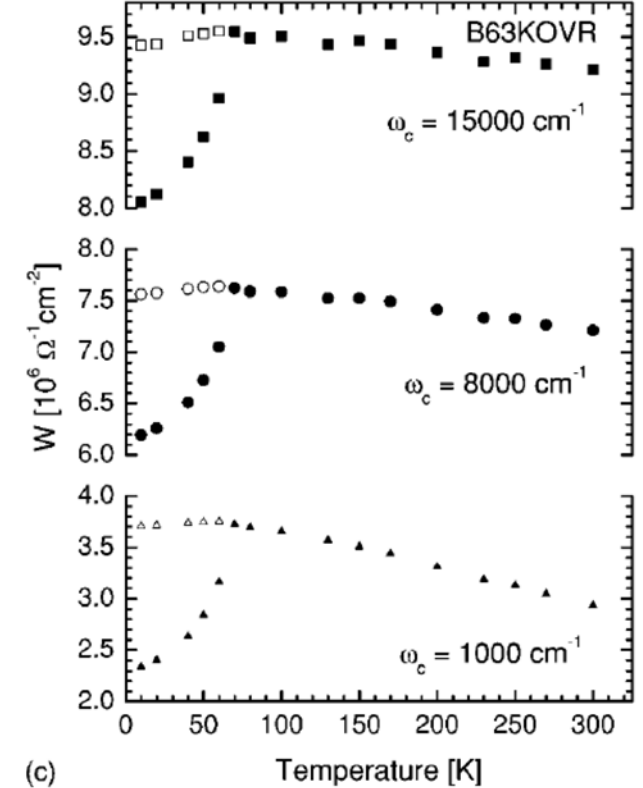
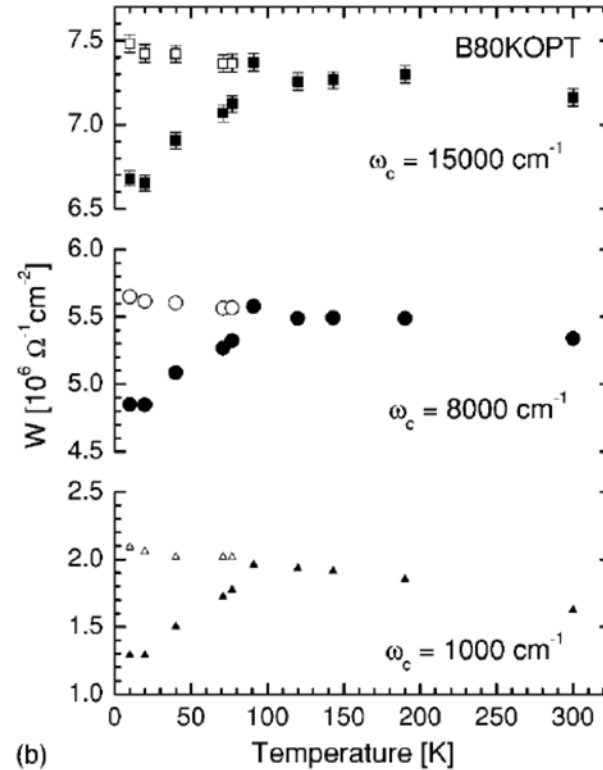
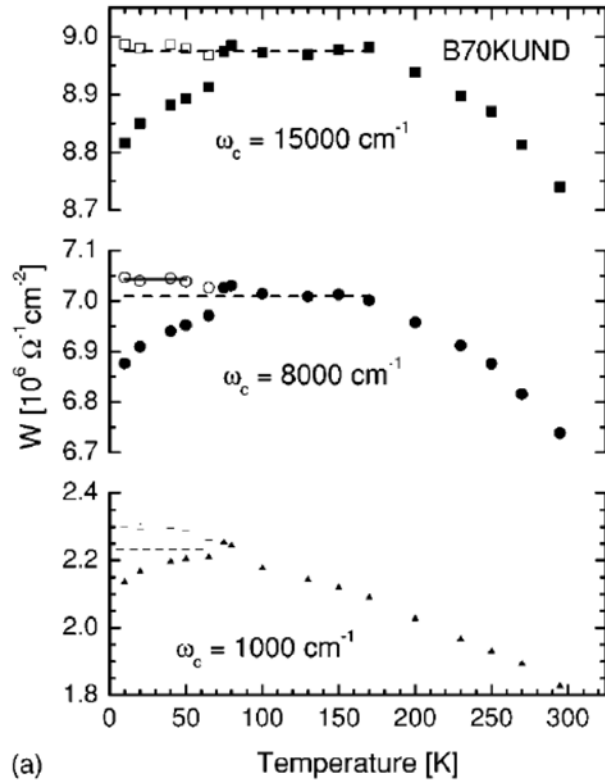
All plots from  
Santander et al.  
Deutscher et al.

FGT sum-rule recovered in underdoped only if integration up to huge scale  $\sim 2\text{-}3 \text{ eV}$  !

# Low/Intermediate-frequency behaviour: non-BCS in UD



# Partial frequency integrations (cutoff $W_c$ )



$$K_{\text{SC}} - K_N = \int_{0^+}^{W_c} d\omega \left[ \sigma_1^{\text{N}} - \sigma_1^{\text{SC}} \right] - \rho_s$$

< 0 in BCS (kinetic energy loss !); >0 if kinetic energy GAIN by going SC

# UD: kinetic energy gain

## OvD: kinetic energy loss (and measurable !)

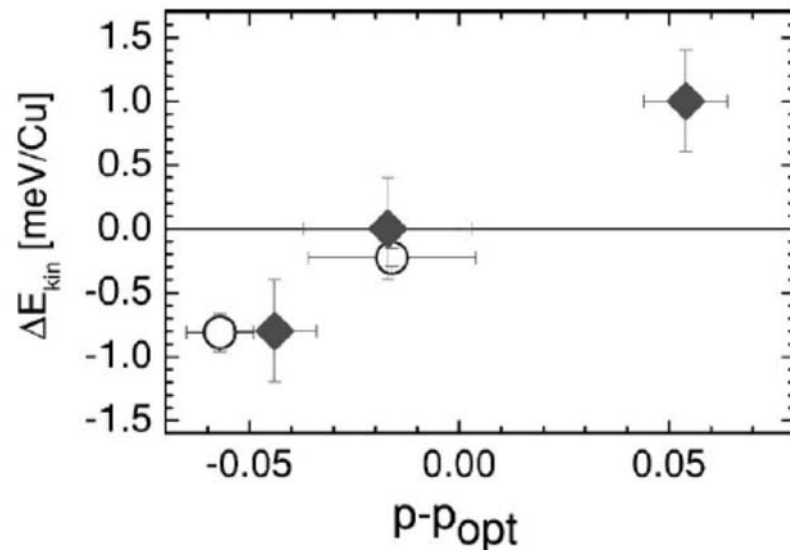
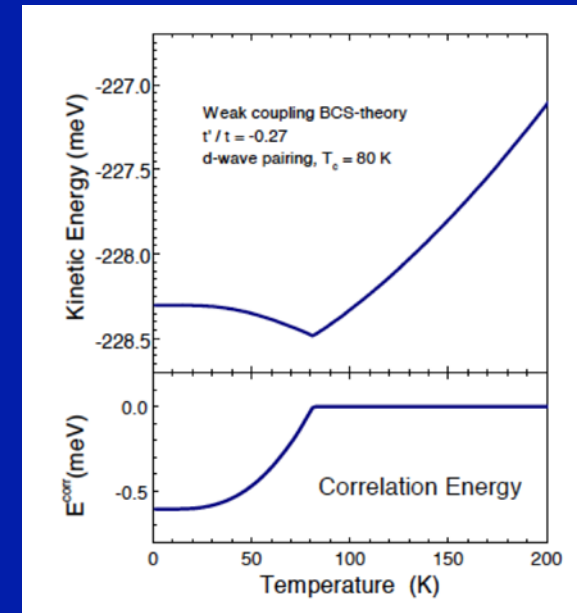


FIG. 2. Change  $\Delta E_{kin}$  of the kinetic energy, in meV per copper site, calculated from Eqs. (1) and (3), vs the charge  $p$  per copper with respect to  $p_{opt}$  [Eq. (6)]. Full diamonds: data from Ref. 3, high-frequency cutoff 1 eV. Open circles: data from Ref. 1, high-frequency cutoff 1.25 eV. Error bars: vertical, uncertainties due to the extrapolation of the temperature dependence of the normal state spectral weight down to zero temperature; horizontal, uncertainties resulting from  $T_c/T_{c,max}$  through Eq. (6) (see text). We have taken  $T_{c,max} = (83 \pm 2)$  K for films and  $(91 \pm 2)$  K for crystals.



$$\frac{\Delta E_{kin}}{E_{kin}^N} \approx \frac{1}{\mathcal{N}(0)\mathcal{V}} \left( \frac{\Delta}{E_F} \right)^2,$$

BCS

# Theory ?

- **Various contributions, see e.g :**
- Kinetic energy loss in BCS vs. gain in BEC for  $U < 0$  Hubbard model:

Toschi, Capone and Castellani, PRB (2006)

Kyung, A.G., Tremblay, PRB (2006)

- t-J model in cluster-DMFT:

Carbone et al. PRB (2006)

(and more...)

## II. Materials dependence of $T_c$ (1): Influence of the number of layers

- General trend:  $T_c$  at optimal doping of given family increases with the number  $n$  of layers (up to  $n=3$ , decreases for larger  $n$ )

Example of Hg-based compounds: Hg-12(n-1)n, up to  $n=5$

Cf. review Antipov et al. Supercond.Sci.Tech. 15, R31 (2002)

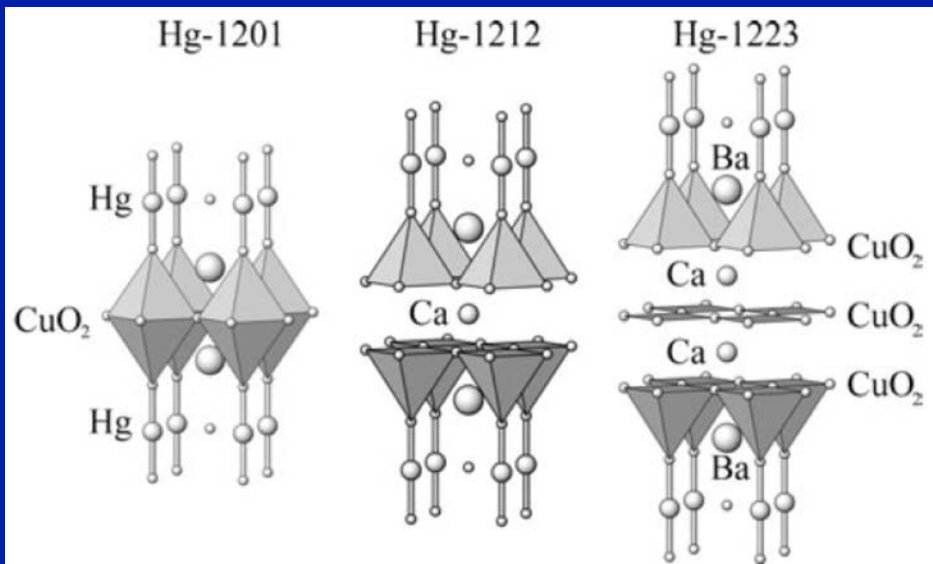


**Figure 10.** Crystal structure of  $\text{HgBa}_2\text{CuO}_{4+\delta}$ ,  $\text{HgBa}_2\text{CaCu}_2\text{O}_{6+\delta}$  and  $\text{HgBa}_2\text{Ca}_2\text{Cu}_3\text{O}_{8+\delta}$ .

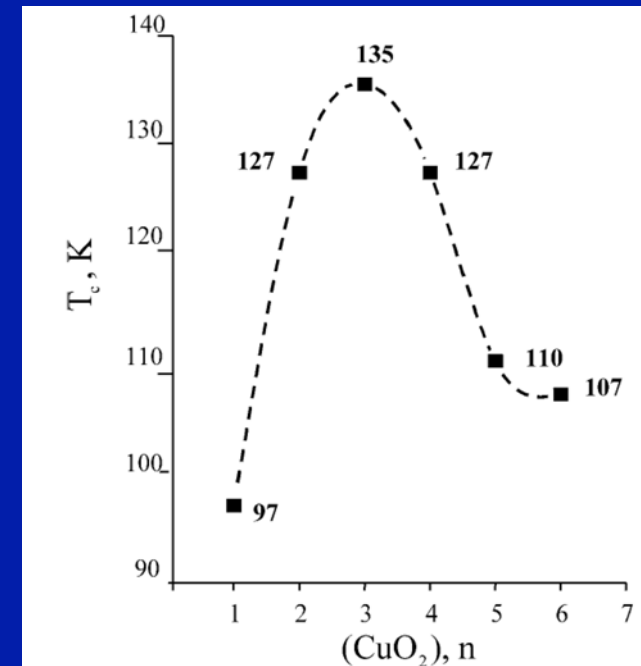


**Figure 15.** The dependence of  $T_c$  versus  $n$  (number of  $\text{CuO}_2$  layers) for  $\text{HgBa}_2\text{Ca}_{n-1}\text{Cu}_n\text{O}_{2n+2+\delta}$ .

# A theory of $T_c$

cf. P.A.Lee et al. Rev Mod Phys (2006) Sec.V

Main message: Both phase fluctuations AND creation of thermally excited (nodal) quasiparticles are important in determining  $T_c$

## 1- Phase fluctuations:

We expect a Berezinskii-Kosterlitz-Thouless transition driven by unbinding of vortex-antivortex pairs. This happens when:

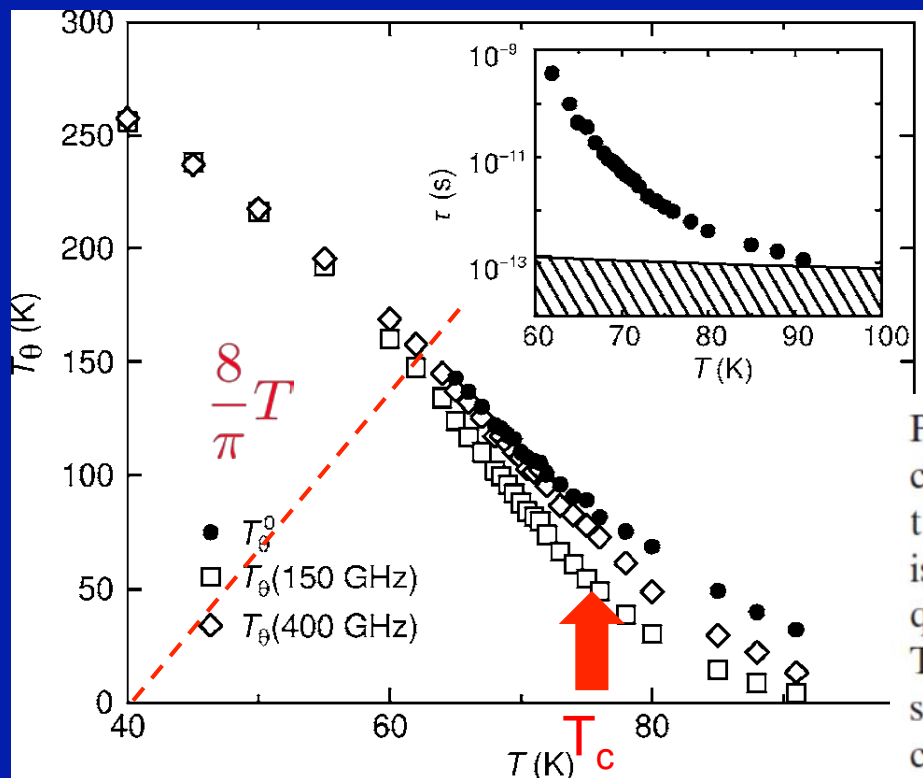
$$\frac{8}{\pi} kT_c = 4K_s(T_c) \equiv \frac{\hbar^2 n_s^{2D}}{m^*}$$

- We have seen that the superfluid stiffness (and superfluid density) at  $T=0$  is reduced by the proximity to the Mott insulator, roughly proportionally to the number of doped holes
- In an n-layer material, the phases in each layer are strongly locked together by interlayer Josephson coupling, hence the n-layer should be considered as a single entity whose phase fluctuates → multiplies by n effective stiffness !

## 2. Thermally excited quasiparticles

We have seen that thermally excited (nodal) quasiparticles yield a depletion of  $K_s(T)$  depending linearly on  $T$  (with a slope  $\sim$  independent of doping level)

All this is confirmed by microwave measurements :



$$T_{\theta}^0 = \frac{\hbar^2 n_s^{2D}}{m^*}$$

Actual  $T_c$  (74K) somewhat larger than BKT (60K) due to 3D ordering

FIG. 16. The phase stiffness  $T_{\theta}$  measured at different frequencies ( $T_{\theta} = \hbar^2 n_s / m^*$ ). The solid dots give the bare stiffness obtained by extrapolation to infinite frequency.  $T_c$  of this sample is 74 K. This is where the phase stiffness measured at low frequency would vanish according to Berezinskii-Kosterlitz-Thouless (BKT) theory. Note the linear decrease of the bare stiffness with  $T$  which extends considerably above  $T_c$ . This decrease is due to thermal excitations of nodal quasiparticles. Inset: The time scale of the phase fluctuation. The hatched region denotes  $\hbar / \tau = kT_c$ . From Corson *et al.*, 1999.

Underdoped Bi2212 – thin films

Including the effect of QPs into the BKT criterion yields:

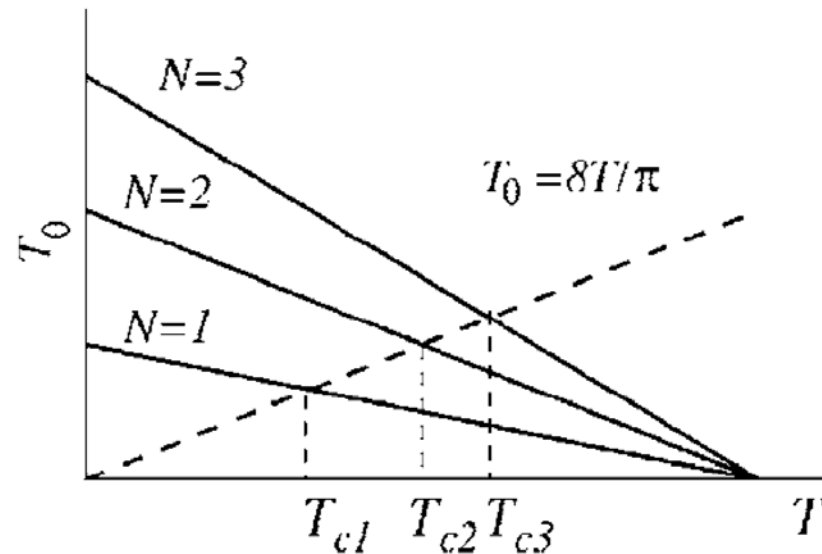


FIG. 17. Schematic plot of the phase stiffness  $T_\theta = \hbar^2 n_s / m^*$  for superconductors with  $N$ -coupled layers. The linear decrease with temperature is due to the thermal excitation of quasiparticles. The transition temperatures  $T_{cN}$ ,  $N=1,2,3$ , are estimated by the interception with the BKT line  $T_\theta = 8T/\pi$ .

# Relationship to isotope effect

- No isotope effect on  $T_c$  observed for optimally doped  $\text{YBCO}_7$
- But significant isotope effect on  $n_s/m^*$  (why ?)
- Isotope effect on both quantities for underdoped (eg  $\text{YPrBCO}$ )

**Table 1.** Summary of the OIE results.

Compound	Method	Sample shape	$\Delta T_c / T_c$ (%)	$\Delta \lambda_{ab}(0) / \lambda_{ab}(0)$ (%)
$\text{YBa}_2\text{Cu}_3\text{O}_{7-\delta}$	LE $\mu$ SR	Thin film	-0.22(16)	2.8(7)
$\text{YBa}_2\text{Cu}_3\text{O}_{7-\delta}$	Magnetization	Fine powder	-0.26(5)	3.0(1.1)
			-0.28(5) <sup>a</sup>	2.4(1.0) <sup>a</sup>
$\text{YBa}_2\text{Cu}_3\text{O}_{7-\delta}$	Bulk $\mu$ SR	Powder	-0.3(1)	2.6(5)
$\text{Y}_{0.8}\text{Pr}_{0.2}\text{Ba}_2\text{Cu}_3\text{O}_{7-\delta}$			-1.3(3)	2.4(7)
$\text{Y}_{0.7}\text{Pr}_{0.3}\text{Ba}_2\text{Cu}_3\text{O}_{7-\delta}$			-2.8(5)	2.5(1.0)
$\text{Y}_{0.6}\text{Pr}_{0.4}\text{Ba}_2\text{Cu}_3\text{O}_{7-\delta}$			-4.6(6)	4.5(1.0)
$\text{La}_{1.85}\text{Sr}_{0.15}\text{CuO}_4$			-1.0(1)	2.2(6)
$\text{Y}_{0.6}\text{Pr}_{0.4}\text{Ba}_2\text{Cu}_3\text{O}_{7-\delta}$	Bulk $\mu$ SR	Site-selective powder	0.1(4) <sup>b</sup>	0.9(5) <sup>b</sup>
			-3.7(4) <sup>c</sup>	3.1(5) <sup>c</sup>
			-3.3(4) <sup>d</sup>	3.3(4) <sup>d</sup>

# Why does $T_c$ decrease in practice for $n > 3$ ?

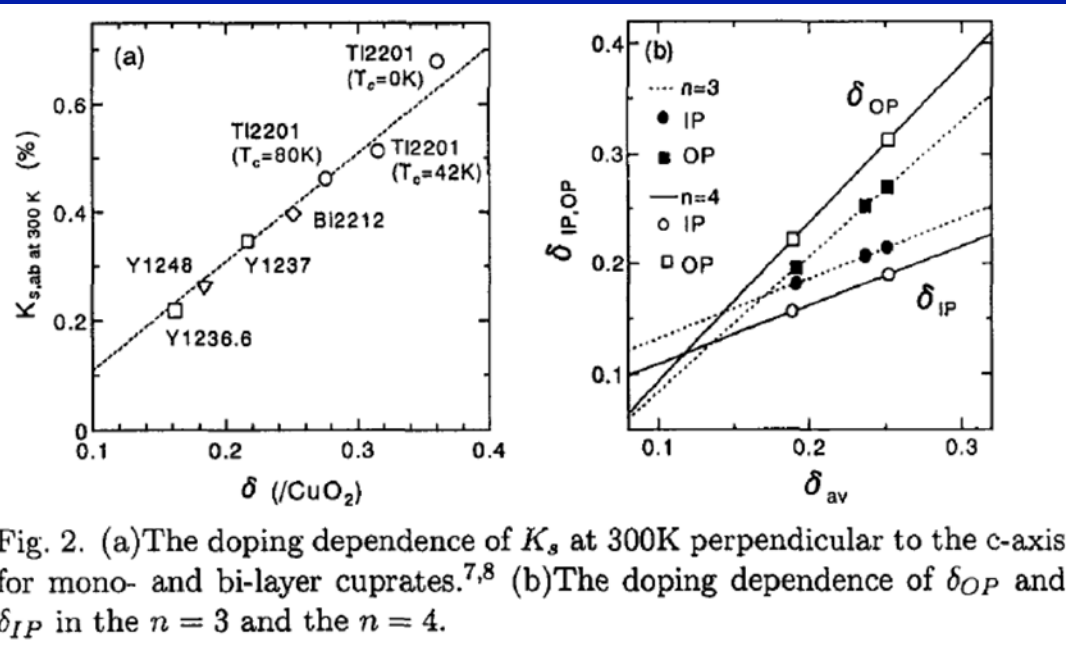


Fig. 2. (a) The doping dependence of  $K_s$  at 300K perpendicular to the c-axis for mono- and bi-layer cuprates.<sup>7,8</sup> (b) The doping dependence of  $\delta_{OP}$  and  $\delta_{IP}$  in the  $n = 3$  and the  $n = 4$ .

Doping becomes inhomogeneous: inner layers become underdoped

Revealed by local probe such as NMR:

cf. Trokiner et al. PRB 1991 Bi2223; Tokunaga et al., JLTP 1999, ...

OP:  
outer planes  
IP:  
Inner plane

$n(n_{IP}/n_{OP})$	3 (1/2)		4 (2/2)	
	Hg1223	Cu1223	Hg1234	Cu1234
$T_c$	115 K	133 K	123 K	117 K
$\delta_{IP}/CuO_2$	0.182	0.207	0.157	0.192
$\delta_{OP}/CuO_2$	0.196	0.252	0.222	0.313
$\delta_{total}$	0.574	0.712	0.758	1.01
$\delta_{IP}(\%) \times n_{IP}$	31.7(%) $\times$ 1	29.1(%) $\times$ 1	20.7(%) $\times$ 2	19.0(%) $\times$ 2
$\delta_{OP}(\%) \times n_{OP}$	34.1(%) $\times$ 2	35.4(%) $\times$ 2	29.3(%) $\times$ 2	31.0(%) $\times$ 2

Table 1. Comparison of the doping concentration between the IP and the OP.

## II. Materials dependence of $T_c$ (2): Influence of next-nearest neighbor hopping $t'/t$ and of coupling to `axial' orbital ?

Question: comparing materials with identical number of layers  $n$ ,  
We see large variations in maximum  $T_c$ . Why ?

e.g. single-layer materials:

Material	LSCO	Bi2201	Tl2201	Hg1201
$T_c$	40	35	~90	~98

Idea proposed by Pavarini et al. PRL 87, 047003 (2001):

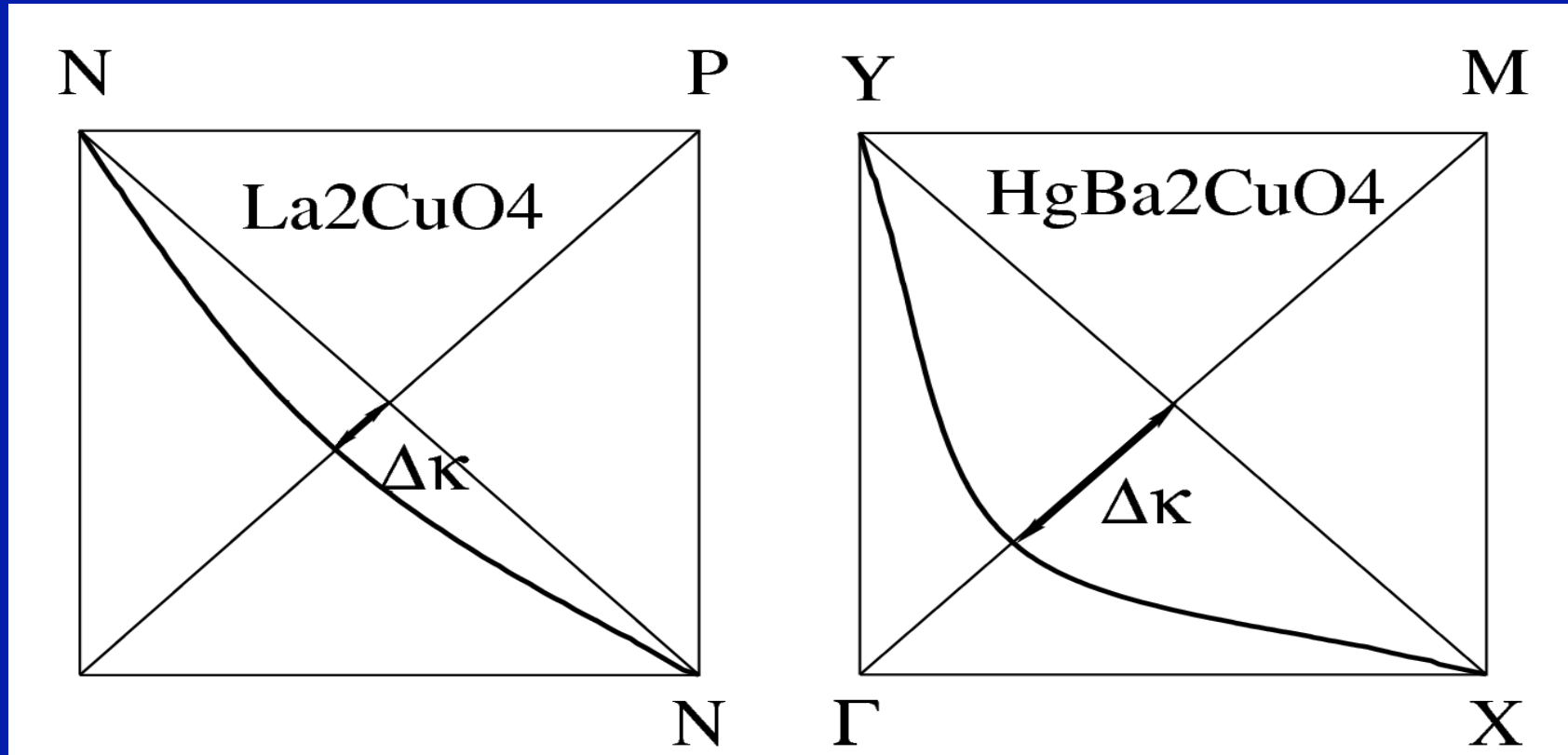
These materials have strong differences in ratio of n.n.n hopping to  
n.n hopping,  $r \sim t'/t$ , which in turn is traced to role of `axial orbital'

(mix of Cu 4s and apical O  $d_{3z^2-r^2}$ )

[ See also for early remarks on importance of  $t'/t$  and apical oxygen:

Raimondi et al. PRB 53, 8774 (1996)]

# Large difference in calculated $t'/t$ between LSCO and Hg1201



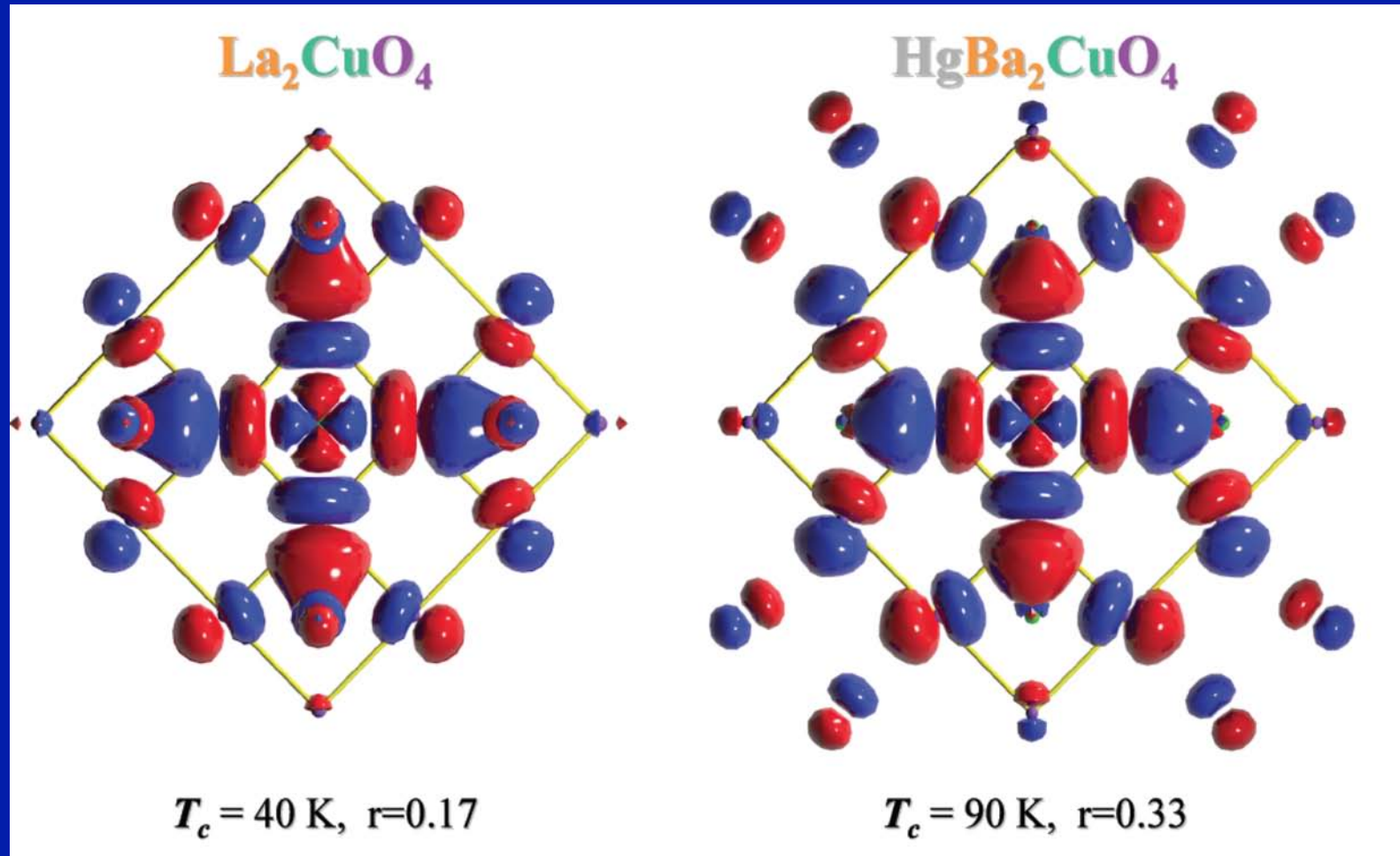
$$T_{c \max} = 40\text{K}, \quad r = 0.17$$

$$T_{c \max} = 90\text{K}, \quad r = 0.33$$

$$r = \frac{1}{2} \sin(\pi \Delta \kappa)$$

Slide borrows from:  
O.K. Andersen, 2010  
private comm.

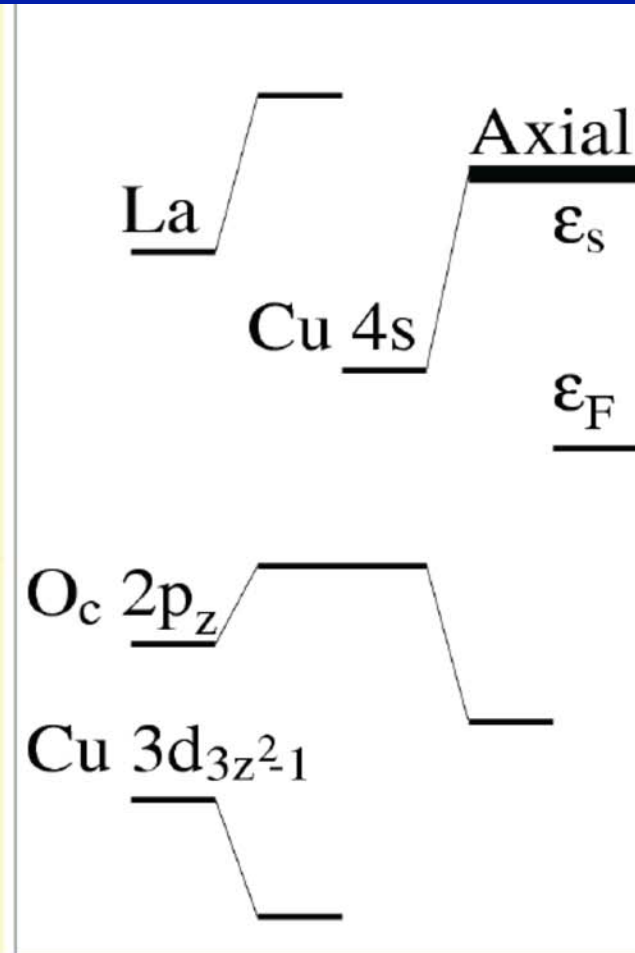
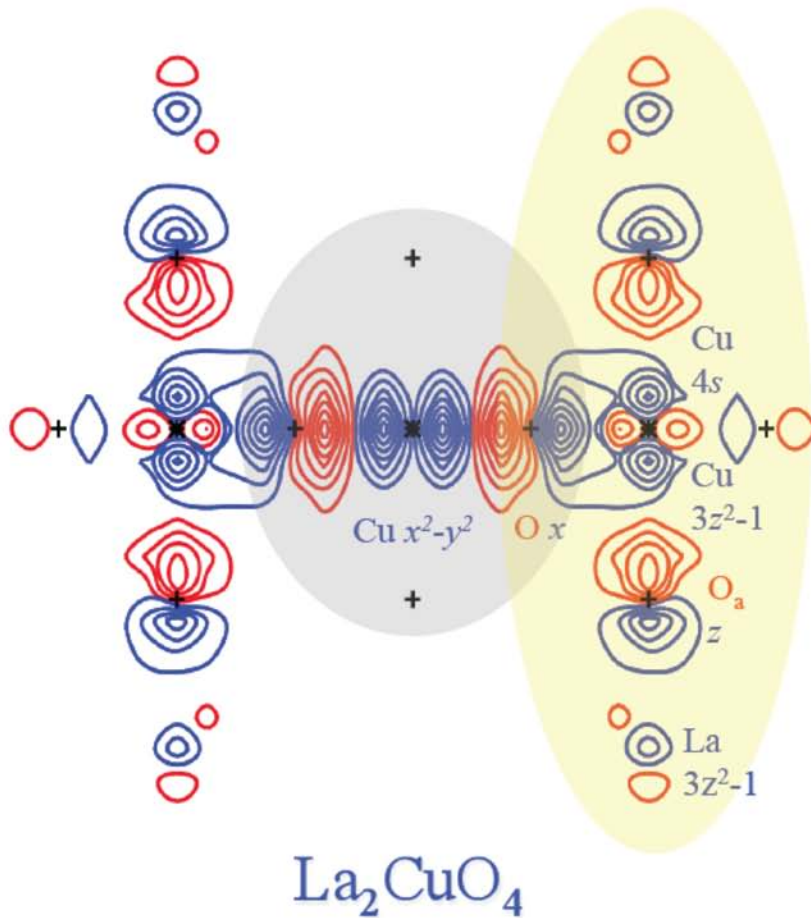
# Comparing Wannier functions:



*Slide borrows from:  
O.K. Andersen, 2010  
private comm.*

# Role of 'axial' orbital in setting $t'/t$

Wannier function for the cuprate conduction band

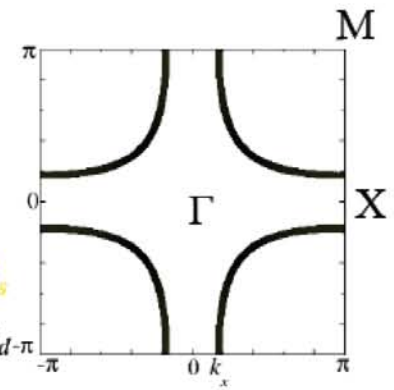
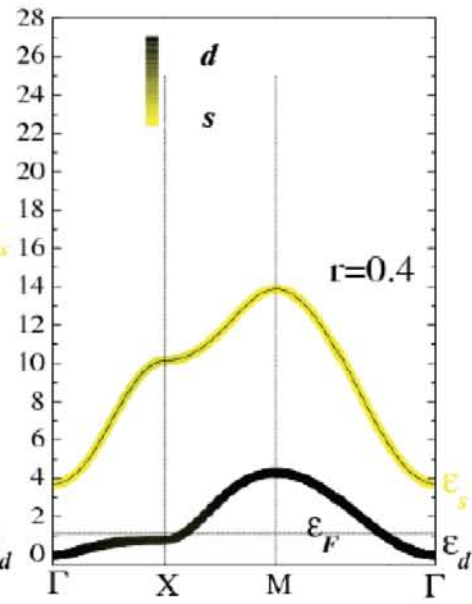
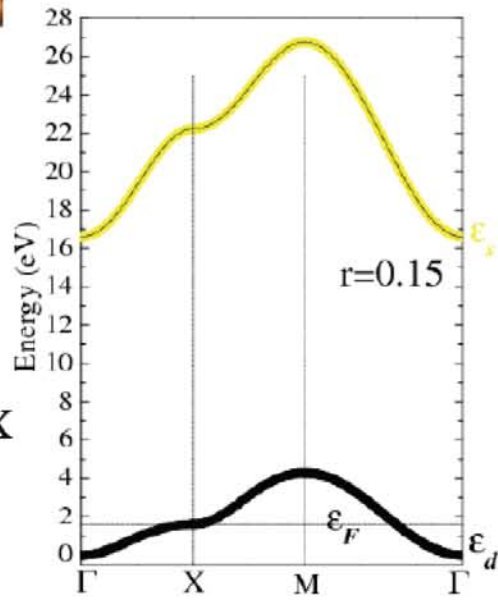
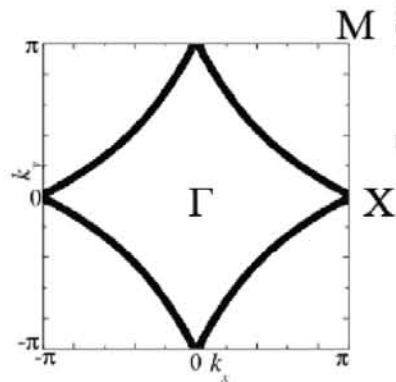
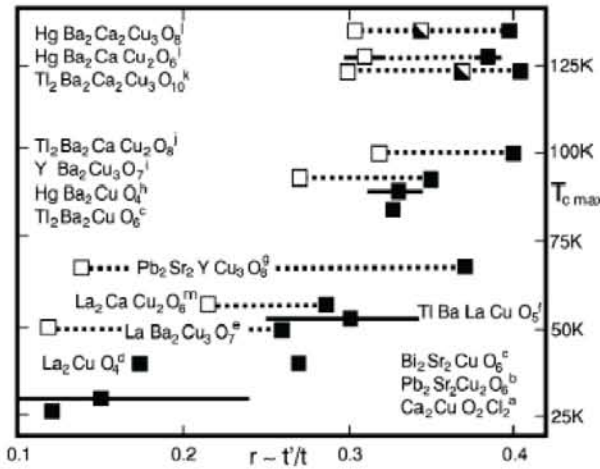
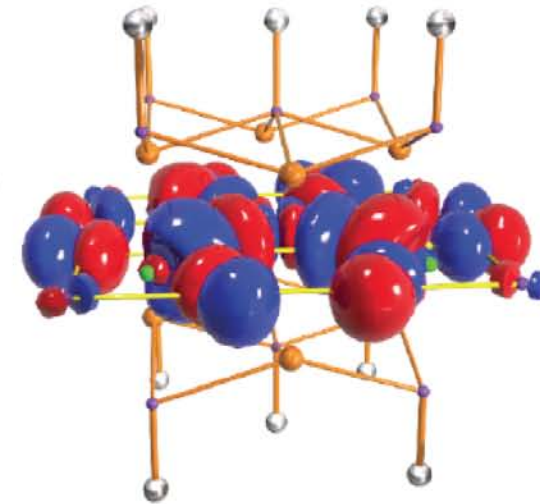
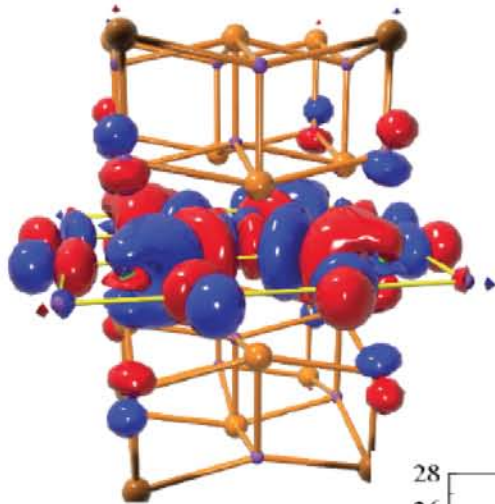


The material-dependent parameter is  $\epsilon_s - \epsilon_F (> 0)$ . The smaller it is, the larger is  $r \sim t'/t$ .

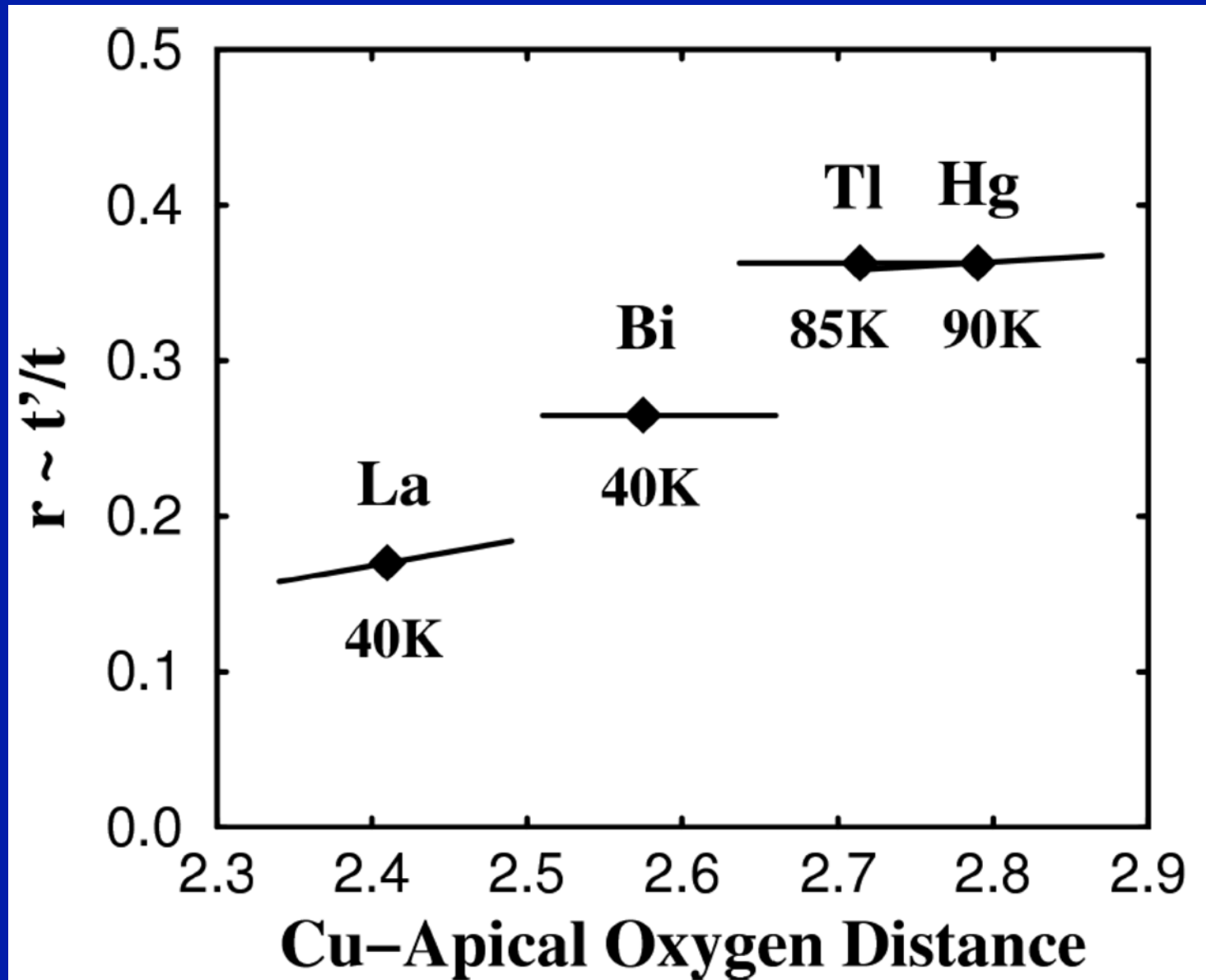
Cuprates  $3d^{9-h} = 3d_{x^2-y^2}^{1-h}$

HgBa<sub>2</sub>CuO<sub>4</sub>

La<sub>2</sub>CuO<sub>4</sub>



Hence,  $t'/t$  increases as apical oxygen is pulled out from the plane



# This trend also applies to n-layer materials

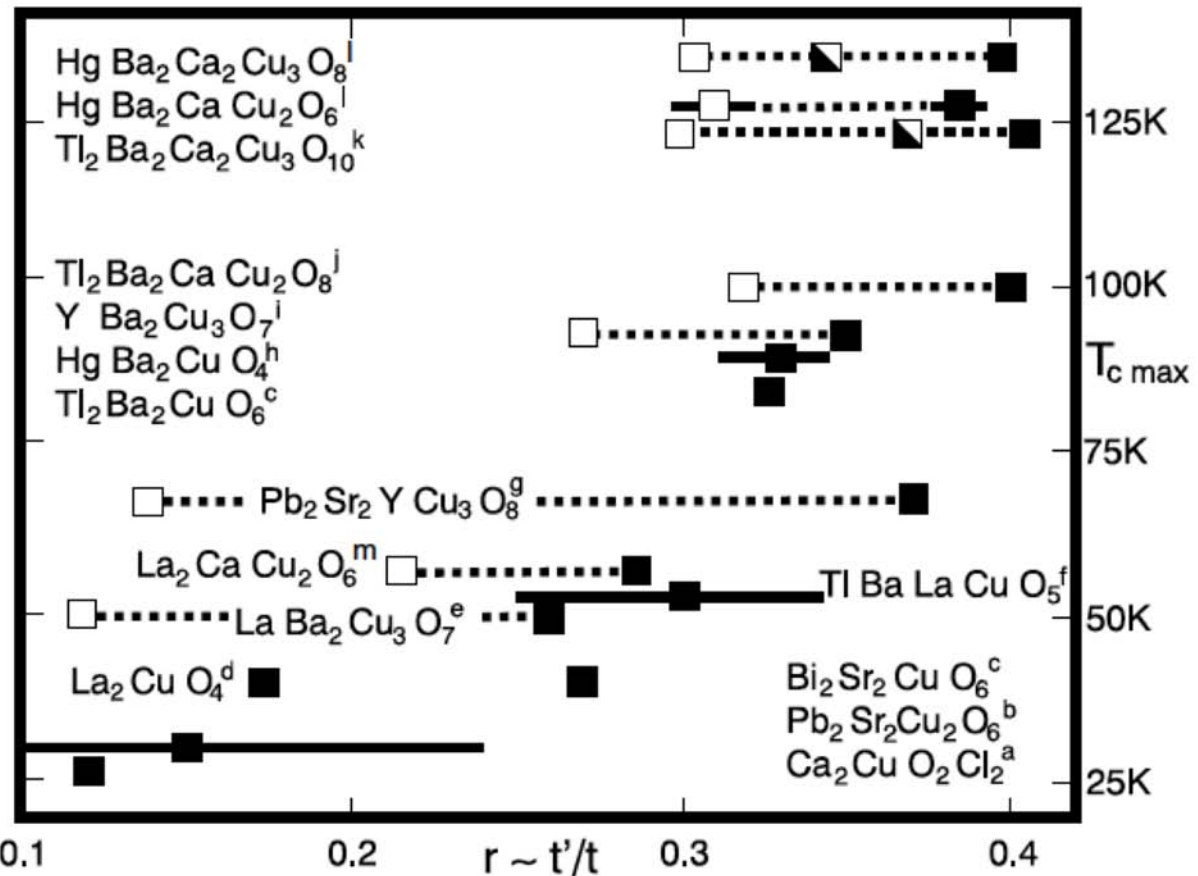


FIG. 5. Correlation between calculated  $r$  and observed  $T_{c \text{ max}}$ . Filled squares: single-layer materials and most bonding subband for multilayers. Empty squares: most antibonding subband. Half-filled squares: nonbonding subband. Dotted lines connect subband values. Bars give  $k_z$  dispersion of  $r$  in primitive tetragonal materials,  $a-m$  [8–20].

# Consistent with ARPES determination of $t'/t$

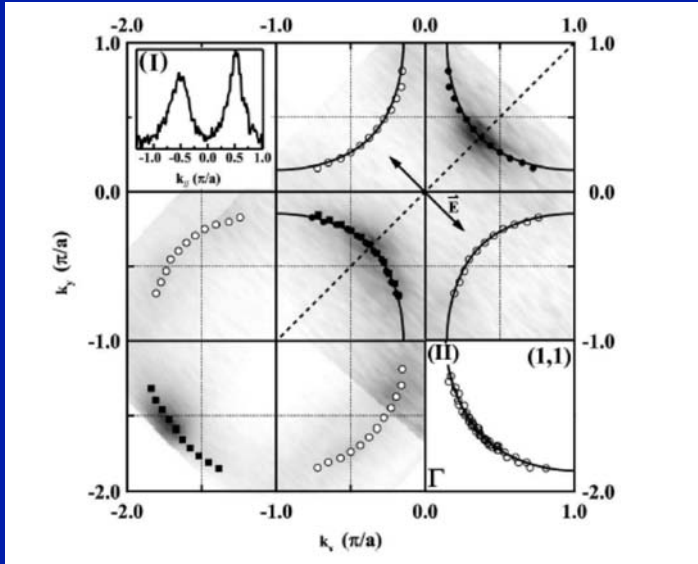


FIG. 3: Fermi surface of the Hg1201 generated by integrating the spectrum  $\pm 10\text{meV}$  with respect to  $E_F$ . The solid symbols represent the Fermi crossing points,  $k_F$ , determined by the peak positions of the MDC near  $E_F$ . The open symbols are symmetrized from the solid symbols. The solid curve is the tight-binding FS as described in the text. The inset (I) shows the MDC around  $E_F$  along the dashed line. The inset (II) illustrates the Fermi crossing points collected from three sets of data which were taken at the SSRL and ALS. The fitted tight binding FS is also shown.

Lee et al. (Shen's group)  
 ArXiv condmat 0606347  
 Hg1201

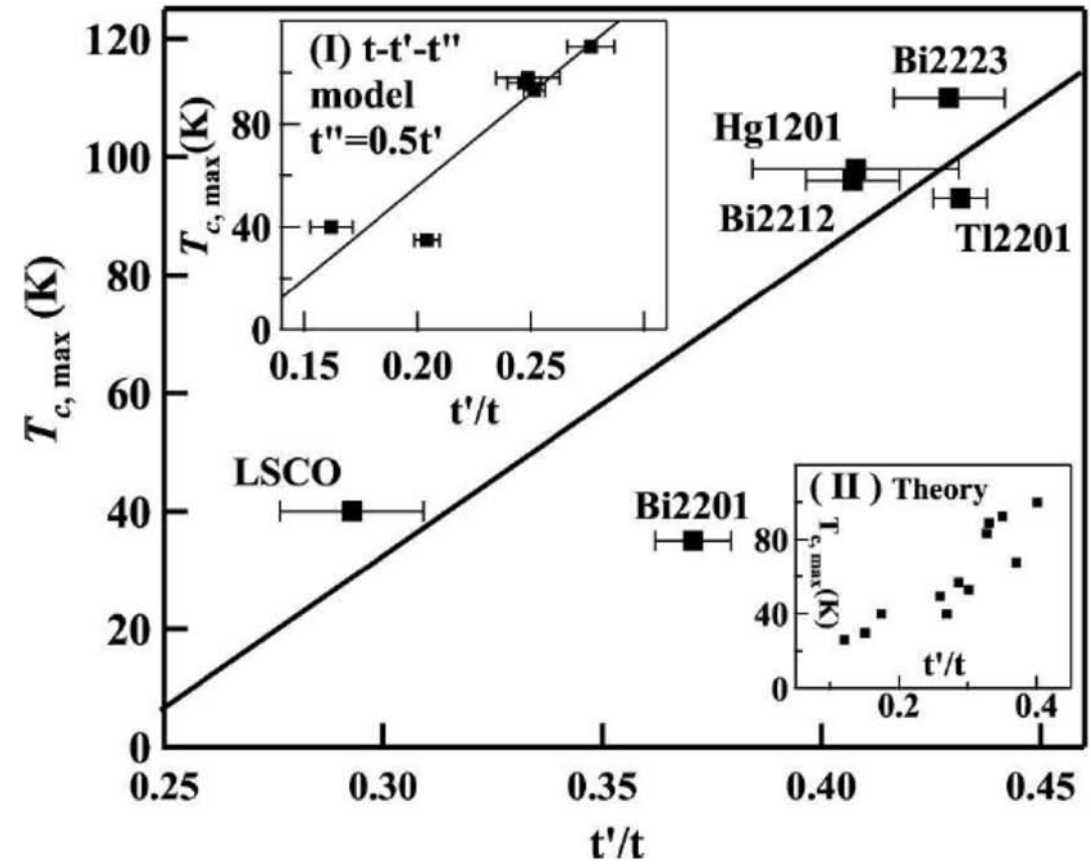
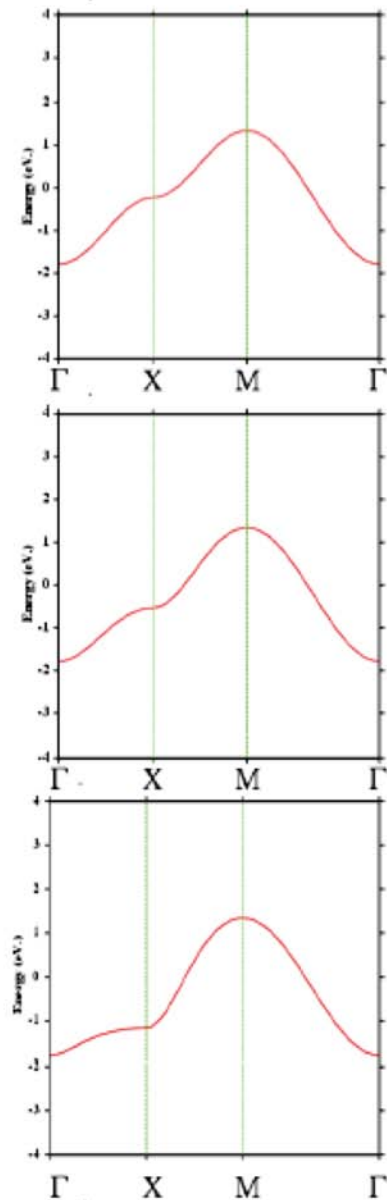


FIG. 4: Positive correlation between  $T_{c,max}$  and  $t'/t$ . Inset (I) is the results obtained from  $t - t' - t''$  model. Error bars are the 99% confidence interval of the fitted  $t'/t$ . Inset (II) is reproduced from Ref.<sup>3</sup>. The lines in the figures are guides-to-the-eye, indicating the positive correlation between  $T_{c,max}$  and  $t'/t$ .

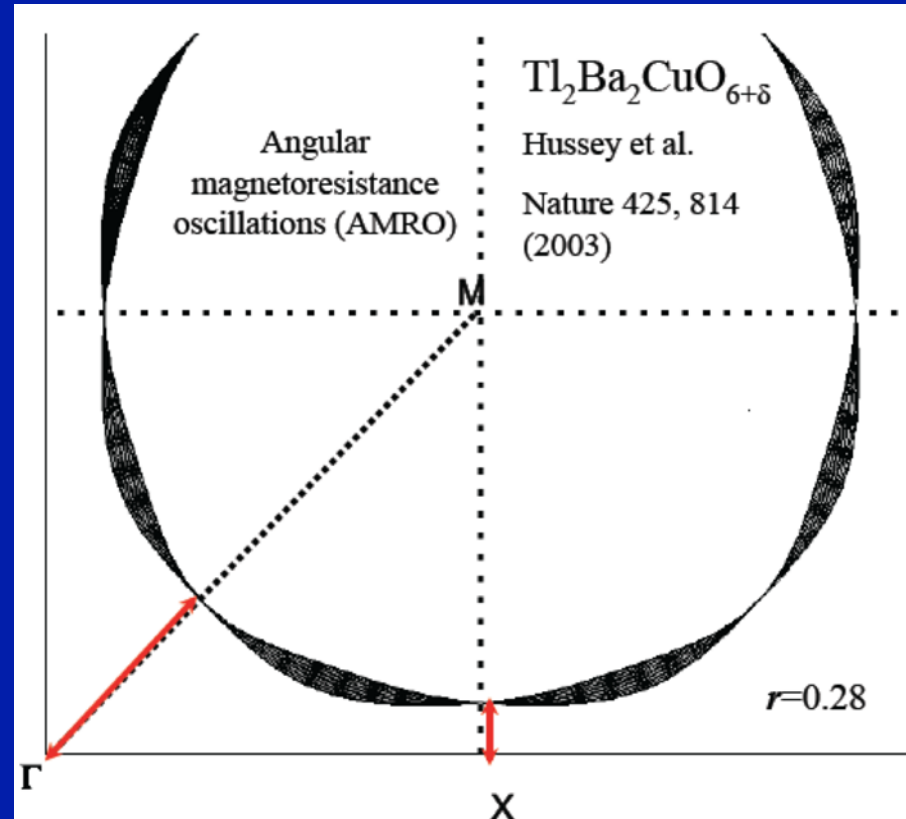
# Also consistent with AMROs on TI-single layer



$r=0$ .

$r=0.1$

$r=0.3$



$$r = \frac{1}{2} \frac{\cos(\pi k_{\Gamma M}/\Gamma M) + \sin^2\left(\frac{\pi}{2} k_{\chi M}/\chi M\right)}{1 - \sin^2\left(\frac{\pi}{2} k_{\chi M}/\chi M\right) [2 + \cos(\pi k_{\Gamma M}/\Gamma M)]}$$

*Slide borrows from: O.K. Andersen, 2010 private comm.*

## II. Materials dependence of $T_c$ (3): influence of apical oxygen distance. [a somewhat confusing issue...]

We have seen that, within the single-layer family,  $T_c$  appears to increase as apical oxygens are pulled out.

However, beautiful recent STM experiments seem to suggest that in 2-layer Bi2212, the local (pseudo ?) gap scale increases as apical oxygens are driven closer to the plane !

Slezak et al. [Davis'group] PNAS 105, 3203 (2008)

This experiment uses to its advantage a well-known 'problem' of Bi2212: lattice mismatch between CuO<sub>2</sub> planes and interplane Blocks, leading to lattice 'supermodulation'

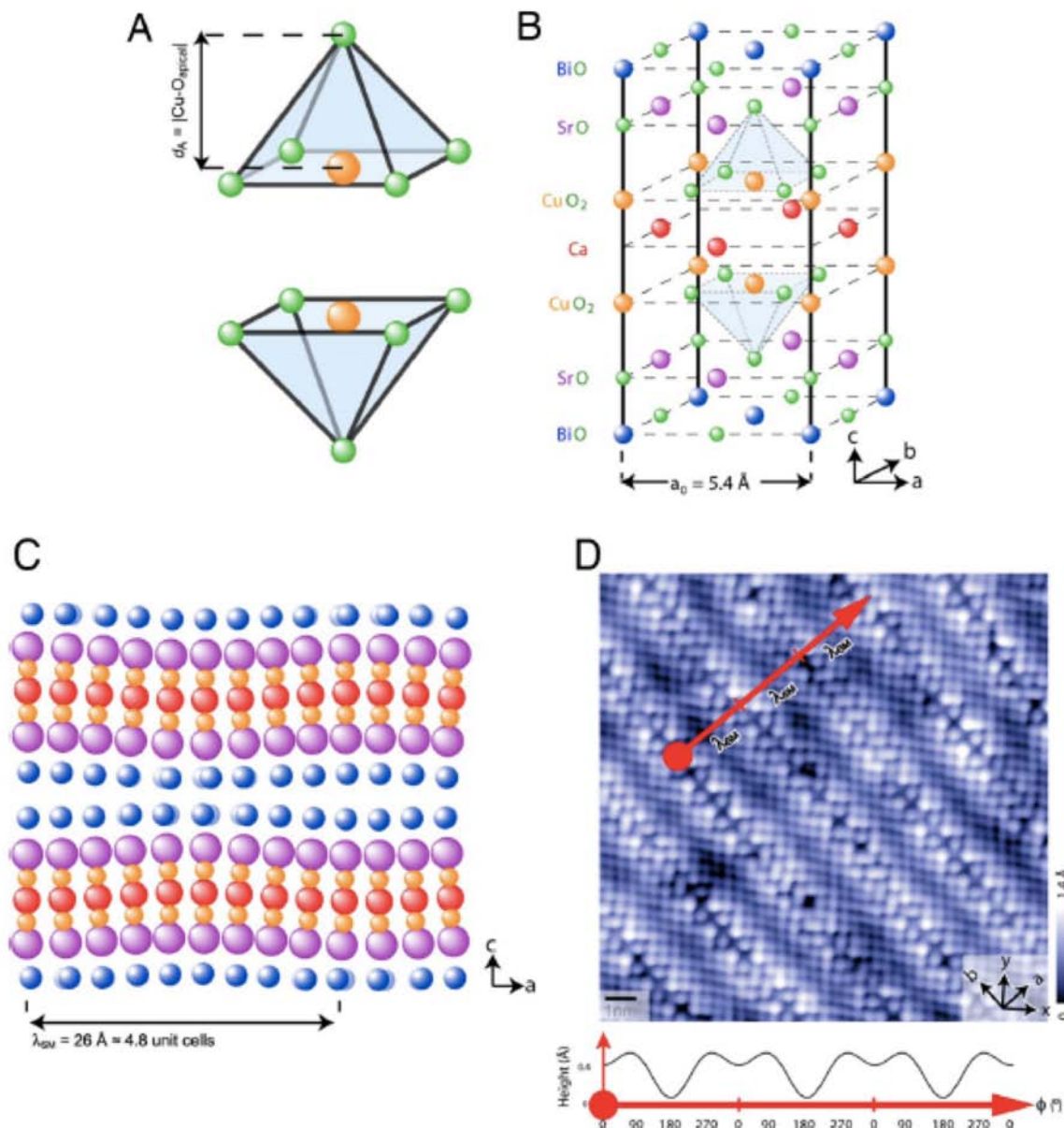


**Fig. 1.** Crystal structure and periodic unit cell distortion due to bulk incommensurate supermodulation. (A) The  $\text{CuO}_5$  pyramidal coordination of oxygen atoms surrounding each copper atom in  $\text{Bi}_2\text{Sr}_2\text{CaCu}_2\text{O}_{8+\delta}$ . (B) Top half of the  $\text{Bi}_2\text{Sr}_2\text{CaCu}_2\text{O}_{8+\delta}$  unit cell (the lower half is identical except for a translation by  $a_0/2$  along the  $a$  axis). Crystal axes  $a$ ,  $b$ , and  $c$  are indicated. (C) Schematic view along the  $b$  axis of the crystal, showing representative displacements of all non-O atoms (adapted from ref. 14). Supermodulation displacements can be seen in both the  $a$  and  $c$  directions. (D) A 14.6-nm-square topographic image of the exposed BiO layer of a cleaved crystal of  $\text{Bi}_2\text{Sr}_2\text{CaCu}_2\text{O}_{8+\delta}$ . The  $x$  and  $y$  axes (aligned along the Cu-O bonds), and the crystalline  $a$  and  $b$  axes, are indicated in the figure. The  $c$  axis supermodulation effect is visible as corrugations of the surface. A simulated cross-section is shown, illustrating the periodic profile of the modulations. [Profile calculated by phase-averaging the topographic height and fitting the first two harmonics of the resulting function  $z(\phi)$ .]

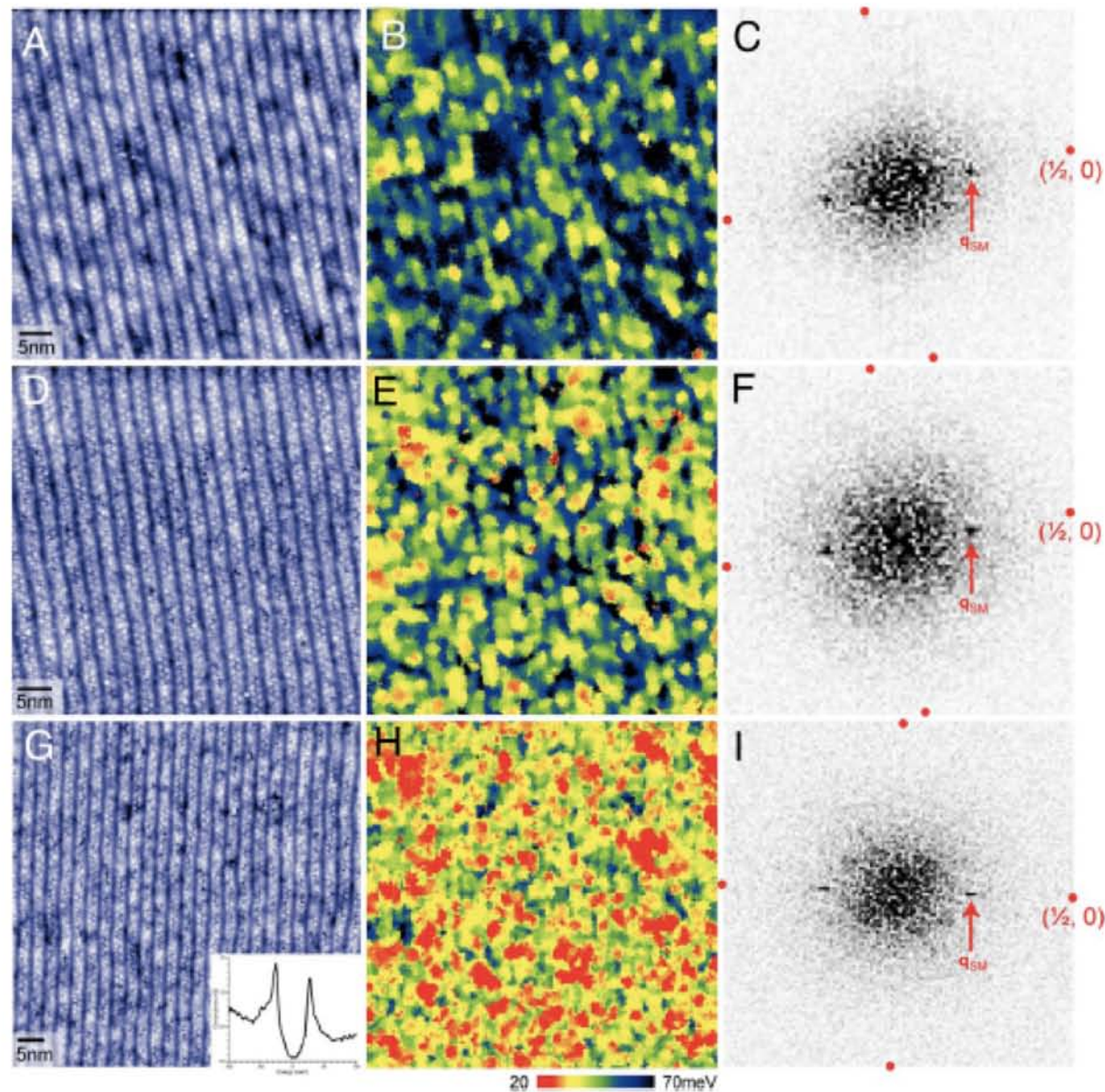
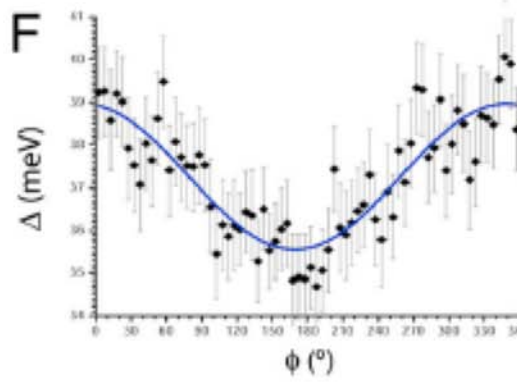
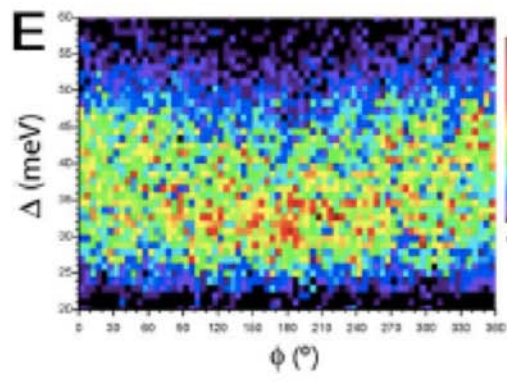
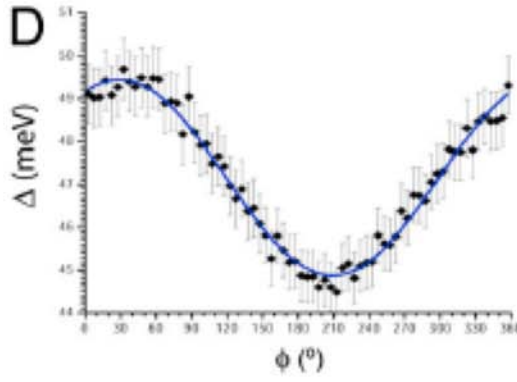
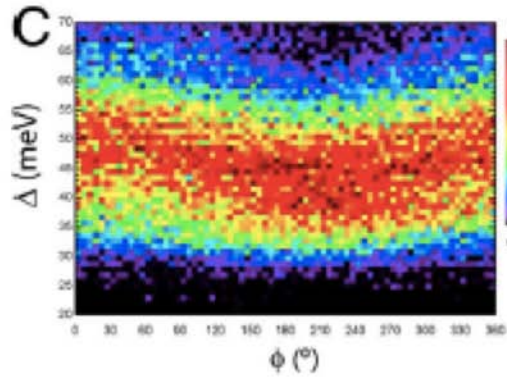
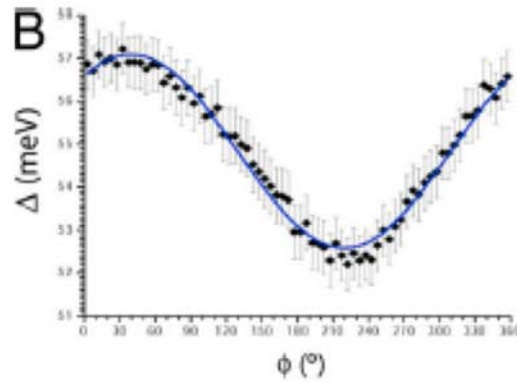
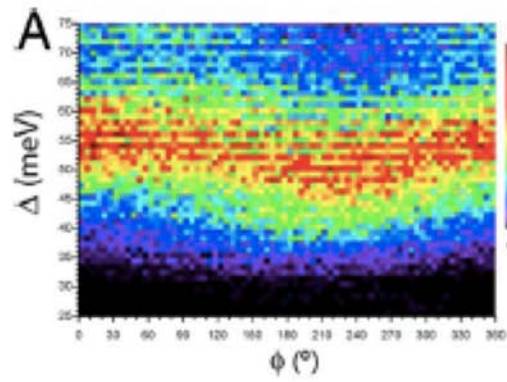


**Fig. 2.** Appearance of gap modulations at the same wavevector  $\mathbf{q}_{SM}$  as the crystal supermodulation. Topographic images of underdoped (mean gap, 5 meV) (A), optimally doped (mean gap, 47 meV) (D), and overdoped (mean gap, 37 meV) (G) samples of  $\text{Bi}_2\text{Sr}_2\text{CaCu}_2\text{O}_{8-\delta}$ . Gap maps B, E, and H correspond to adjacent topographs A, D, and G, respectively, alongside their respective Fourier transforms C, F, and I. Clear peaks are visible in the Fourier-transformed gap maps at  $\mathbf{q}_{SM}$  (indicated). Points corresponding to  $(\pm\frac{1}{2}, 0)$  and  $(0, \pm\frac{1}{2})$  are indicated, in units of  $2\pi/a_0$ .



“Pair density wave”

From structural studies, the modulation has a known correlation to apical oxygen height

# Theoretical understanding: ?

There have been various theoretical attempts at addressing these material-dependent aspects, but no widely accepted view yet I believe...

See e.g. :

- Ohta et al. PRB 43 2968 (1991)
  - Yang et al. PRB 76 100501(R) 2007
  - Mori et al. PRL 101 247003 (2008)
  - Kent et al. PRB 78 035132 (2008)
- and surely many others...

## Other structural aspects: pressure studies: $T_c$ dependence on $a$ -parameter

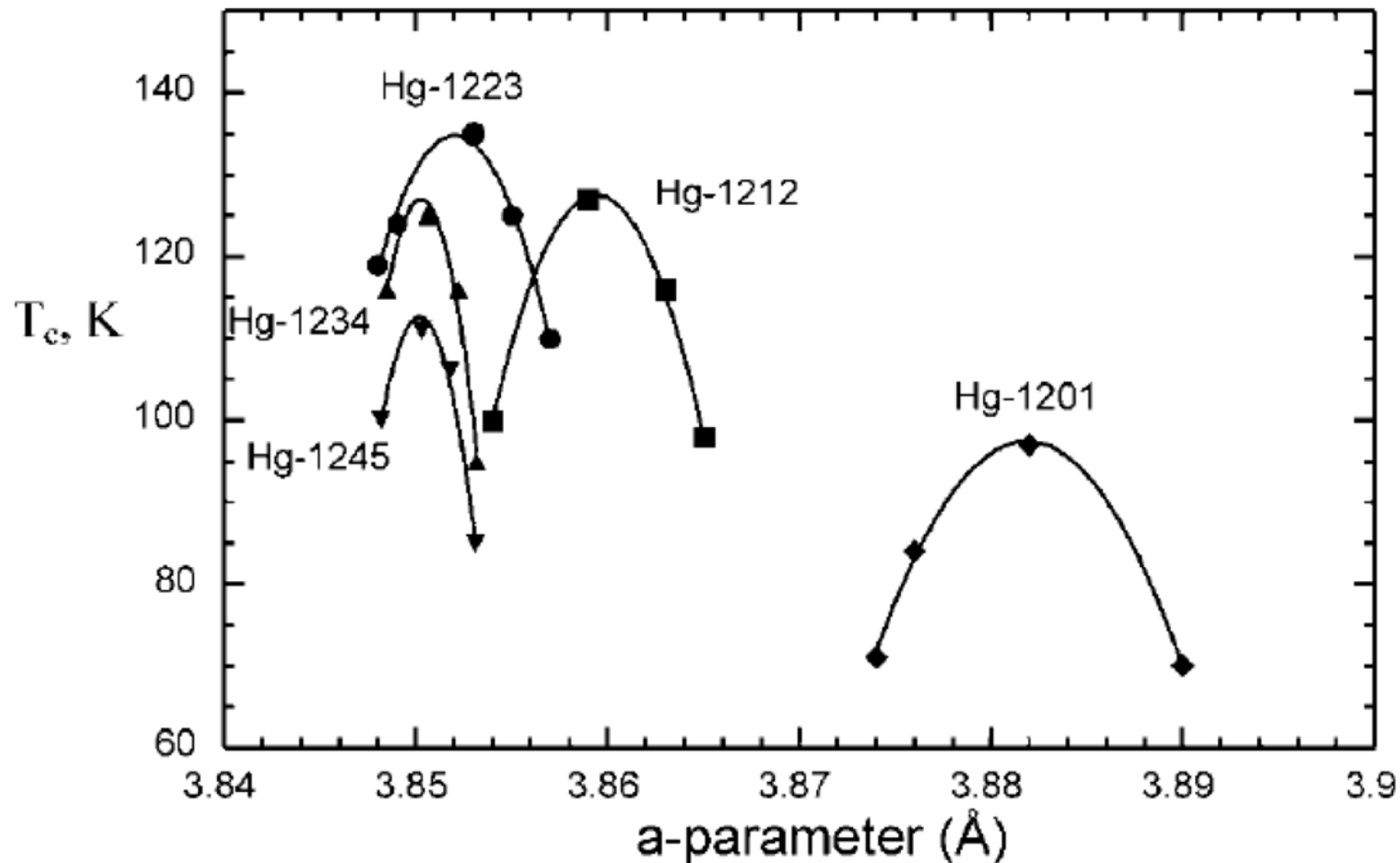


**Figure 16.** The dependence of  $T_c$  versus  $a$ -parameter for the  $\text{HgBa}_2\text{Ca}_{n-1}\text{Cu}_n\text{O}_{2n+2+\delta}$  series.

III. What is the underlying (normal-state ?)  
'fermiology' on which the SC state is built ?

... the surprises of quantum oscillation  
experiments → Cyril Proust's seminar